DOI: 10.1002/chem.201100216

Chemical Modulation of Peptoids: Synthesis and Conformational Studies on Partially Constrained Derivatives

Alejandra Moure,[a] Glòria Sanclimens,[a] Jordi Bujons,[b] Isabel Masip,[a] Angel Alvarez-Larena,[c] Enrique Pérez-Payá,[d] Ignacio Alfonso,[b] and Angel Messeguer*[a]

Dedicated to Professor Josep Font on occasion of his 70th birthday

Abstract: The high conformational flexibility of peptoids can generate problems in biomolecular selectivity as a result of undesired off-target interactions. This drawback can be counterbalanced by restricting the original flexibility to a certain extent, thus leading to new peptidomimetics. By starting from the structure of an active peptoid as an apoptosis inhibitor, we designed two families of peptidomimetics that bear either 7-substituted perhydro-1,4-diazepine-2,5-dione **2** or 3-substituted 1,4-piperazine-2,5-dione **3** moieties. We report an efficient, solid-phase-based synthesis for both peptidomimetic families **2** and **3** from a common intermediate. An NMR spectroscopic study of **2a**,**b** and **3a**,**b** showed two species in solution in different solvents that interconvert slowly on the NMR timescale. The *cis*/*trans* isomerization around the exocyclic tertiary amide bond is responsible for this conformational behavior. The *cis* isomers are more favored in nonpolar environments, and this preference is higher for the six-membered-ring derivative **3a**,**b**. We propose that the hydrogen-bonding pattern could play an important role in the *cis*/*trans* equilibrium process. These hydrogen bonds were characterized in solution, in the solid state (i.e., by using X-ray studies), and by molecular modeling of simplified systems. A comparative study of a model peptoid **10** containing the isolated tertiary amide bond under study outlined the importance of the heterocyclic moiety for the prevalence of the *cis* configuration in **2a** and **3a**. The kinetics of the *cis*/*trans* interconversion in **2a**, **3a**, and **10** was also studied by variable-temperature NMR spectroscopic analysis. The full line-shape analysis of the NMR spectra of **10** revealed negligible entropic contribution to the energetic barrier in this conformational process. A theoretical analysis of **10** supported the results observed by NMR spectroscopic analysis. Overall, these results are relevant for the study of the peptidomimetic/biological-target interactions.

Keywords: conformation analysis · heterocycles · NMR spectroscopy · peptidomimetics · solid-phase synthesis

Introduction

Oligomers of *N*-substituted glycines (peptoids) were introduced by Bartlett and co-workers as a distinctive family of peptidomimetics.[1] The availability of peptoids as individual compounds rationally designed to address a defined target or as libraries of controlled mixtures (constructed under a split-pool or positional-scanning format) made them attractive for high-throughput screening programs.[2] In this context, the development of a convenient modular synthesis for their generation (i.e., the submonomer approach) makes possible the introduction of a wide chemical diversity at the nitrogen atom of the glycine moiety.[3] In comparison with peptides, it was anticipated that peptoids might exhibit higher resistance to the action of proteases as well as improved cellular-uptake features.[4] As a result, interesting bioactive compounds as ligands for pharmaceutically targets, such as G-protein-coupled receptors,[5] urokinase receptor,[6] SH3 domains of signaling proteins,[7] HDM2 protein,[8] neutralizers of bacterial endotoxins,[9] antimicrobial agents,[10] antagonists of TRPV1 channel,[11] lung surfactants,[12] and

[a] Dr. A. Moure, Dr. G. Sanclimens, Dr. I. Masip, Prof. Dr. A. Messeguer
Department of Chemical and Biomolecular Nanotechnology
Instituto de Química Avanzada de Cataluña
Consejo Superior de Investigaciones Científicas
J. Girona, 18, 08034 Barcelona (Spain)
Fax: (+34) 932045904
E-mail: angel.messeguer@cid.csic.es

[b] Dr. J. Bujons, Dr. I. Alfonso
Department of Biological Chemistry and Molecular Modeling
Instituto de Química Avanzada de Cataluña
Consejo Superior de Investigaciones Científicas
J. Girona, 18, 08034 Barcelona (Spain)

[c] Dr. A. Alvarez-Larena
Servicio de Difracción de Rayos X
Universidad Autónoma de Barcelona
08193 Cerdanyola (Spain)

[d] Prof. Dr. E. Pérez-Payá
Laboratory of Peptide and Protein Chemistry
Centro de Investigación Príncipe Felipe
46012 Valencia (Spain)

Supporting information for this article is available on the WWW under http://dx.doi.org/10.1002/chem.201100216.

drug and gene delivery agents,[13] among others, have been identified.

From a structural point of view, although peptoids can adopt secondary structures depending on their size and the residues linked to the nitrogen atoms on the backbone,[14] in general they are highly flexible molecules. In peptoids, the *cis* conformation of the amide bonds that connect the monomer residues can be more highly populated than in peptides.[15] Nevertheless, not all the *cis*/*trans* conformational isomers of the different amide bonds present in a defined peptoid will be biologically active in front of a specific target. By taking advantage of the intensive research into short peptoids as a result of their potential application in drug discovery, Borchardt and Rabenstein recently reported the use of NMR spectroscopic techniques to study *cis*/*trans* isomerization by rotation around the amide bonds of small peptoid models.[16] These authors observed a slow *cis*/*trans* exchange rate for even the most labile of the amide bonds between the two C-terminal residues. This feature can be of importance with respect to the on/off rates for the ligand/receptor binding or when facing undesired interactions with other targets. In parallel studies related to the structural requirements of peptoids for biological function, Blackwell and co-workers explored interactions between the amide bonds and different aromatic side chains, thus concluding that modulation of the $n\rightarrow\pi^*$ effects can alter the ratio of *cis*/*trans* amide bond conformers.[17]

In connection with our interest on the biological activity of peptoids, it is now well established that multiprotein complexes are important points of regulation in cellular-signaling pathways, thus raising attention as targets for the development of chemical modulators. Peptoids features are attractive for application to the modulation of proteins[8,10,18] as well as protein/protein interactions. In this context, programmed cell-death mechanisms (apoptosis) constitute an example of the pivotal interest in controlling different pathologies.[19] We previously reported that a medium-throughput screening of a positional-scanning combinatorial library of *N*-alkylglycine trimers[20] allowed the identification of peptoid **1a** (Scheme 1) as an inhibitor of the apoptosome-dependent activation of procaspase-9.[21] In this context, we also identified peptoids as pharmacological inhibitors of noncanonical polyubiquitylation; these compounds compete with ubiquitin E2 variant (UEV) for its interaction with UBC13 and inhibit its enzymatic activity.[22]

However, in contrast with the wide possibilities of identifying hits against pharmaceutical targets, the high conformational flexibility of peptoids can generate selectivity problems because of undesired off-target interactions. This drawback can be counterbalanced by a second generation of peptidomimetics in which the original conformational flexibility could be restricted to a certain extent. The structural simplicity of peptoids makes them amenable to chemical modulation, thus facilitating the optimization of hit molecules for druglike properties.[23] We deemed that the formal cyclization through selected points of the peptoid molecule would lead to constrained analogues that could improve their potency and selectivity. Moreover, if our approach successfully identified more potent modulators of apoptotic protease activating factor 1 (Apaf-1), these molecules, being conformationally more restricted, could be useful for defining more precisely the interaction that takes place with the protein target.

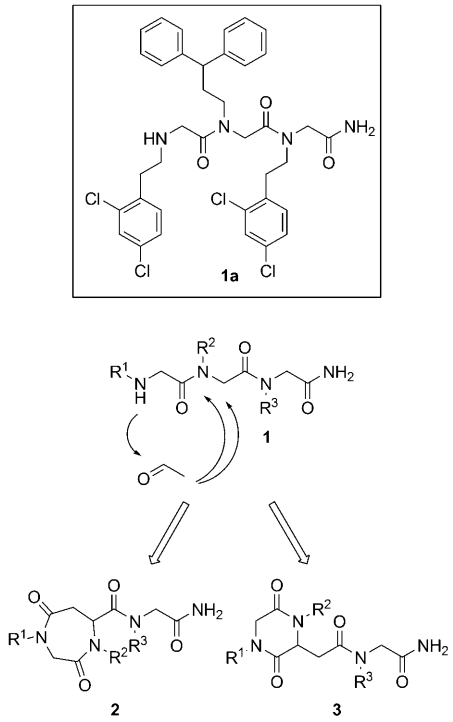

Scheme 1. Peptoid **1a** has been identified as an inhibitor of the formation of the apoptosome and the formal chemical modulation of **1** to generate constrained heterocyclic analogues **2** and **3**.

Covalent constraints have been explored in peptoid research mainly by employing macrocyclization between side chains,[24] head-to-tail strategies,[25] or Ugi four- and three-component reactions.[26] In our case, from the different possibilities contemplated to obtain constrained peptidomimetics derived from the identified peptoid hits, those approaches that generated the novel 7-substituted perhydro-1,4-diazepine-2,5-dione **2** and 3-substituted 1,4-piperazine-2,5-dione **3** derivatives were selected (Scheme 1). In these systems, two of the three tertiary amide bonds present in the molecules are forced to adopt the *cis* configuration by the heterocycle formation. Both **2a** and **3a** were shown to be potent inhibitors of the apoptosome formation and capable of decreasing cell death in different cellular models of apoptosis.[27] Furthermore, **2b** and **3b** are potent inhibitors of noncanonical polyubiquitylation and produce significant biological effects with potential therapeutic applications in cancer and inflammation areas.[22,28]

We report herein on an efficient solid-phase-based synthetic approach to the peptidomimetic families **2** and **3**. In addition, an NMR-based structural study of **2a** and **3a** in different solvents was carried out to determine the thermo-

dynamic and kinetic parameters that define the relative stability of the *cis*/*trans* conformers potentially present around the exocyclic amide bond. Such an amide bond is the only one that still shows conformational flexibility relative to the original peptoid hit. To the best of our knowledge, there are no precedents on structural studies on these families of peptidomimetics. In addition to our general interest in studying the influence of the frozen *cis* configuration around the two amide bonds on the exocyclic bond, we anticipated that this structural study would be highly useful for a better understanding of the interaction between the peptidomimetics with the biological target, thus giving more precise information for the design of improved compounds.

Results and Discussion

Synthesis of compounds 2 and 3: We developed a route for the synthesis of 7-substituted perhydro-1,4-diazepine-2,5-dione **2** and 3-substituted 1,4-piperazine-2,5-dione **3** derivatives (Scheme 1) from the common intermediate **6** (Scheme 2). The compounds were synthesized by using solid-phase chemistry. A solid support shows several indisputable advantages over solution chemistry: purification is facilitated by simple filtration, thus avoiding time-consuming separation techniques; subsequent building blocks and reagents can be added in excess to drive reactions to completion; and the "pseudo-dilution effect", which is the result of using the polymeric solid support, makes intramolecular cyclization a suitable reaction that could be carried out efficiently on solid phase rather than in solution. Additionally, the pro-

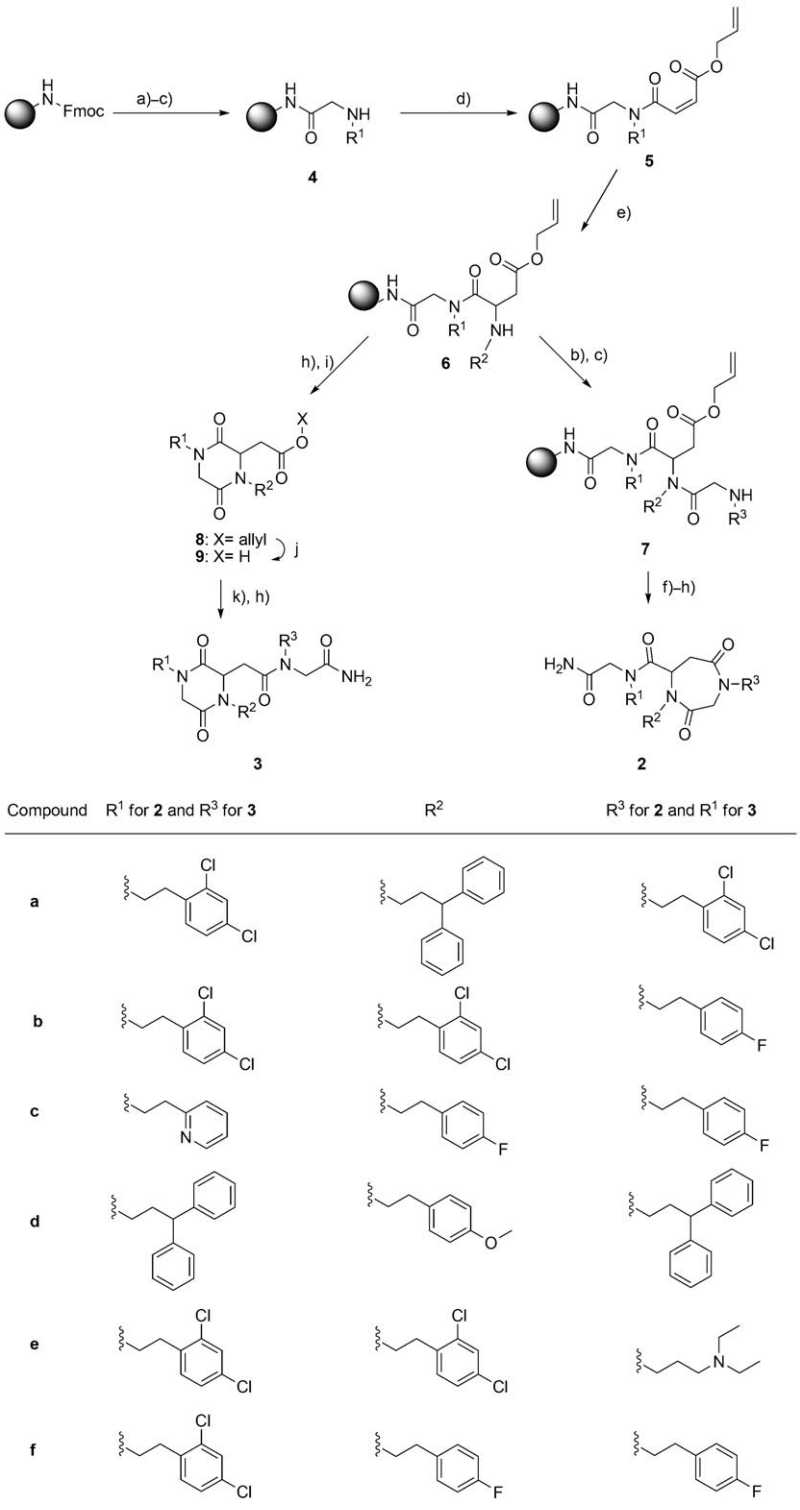

Scheme 2. Solid-phase synthesis of the conformationally restricted peptidomimetics **2** and **3**. a) Piperidine 20%, DMF, MW 2 min at 60°C; b) $BrCH_2COOH$, DIC, DMF/CH_2Cl_2, MW 1 min at 35°C; c) RNH_2, Et_3N, DMF, MW 2 min at 90°C; d) allyl maleate, HOBt, DIC, DMF/CH_2Cl_2, MW 1 min at 45°C; e) RNH_2, Et_3N, DMF, 16 h, RT; f) 0.5 N KOH, dioxane 1:3, MW 4 min at 110°C; g) PyBOP, HOBt, DIPEA, DMF, 20 min at 60°C; h) TFA/CH_2Cl_2/H_2O, 30 min, RT; i) dioxane, MW 4 min at 120°C; j) 4 N NaOH, allyl alcohol, dioxane, MW 4 min at 90°C; k) peptoidyl-resin **4**, HOBt, DIC, DMF/CH_2Cl_2, 3 h at RT. DIC = *N*,*N*′-diisopropylcarbodiimide, DIPEA = diisopropylethylamine, Fmoc = 9-fluorenylmethoxycarbonyl, HOBt = 1-hydroxybenzotriazole, MW = microwave, PyBOP = benzotriazole-1-yloxy-tris-pyrrolidinophosphonium hexafluorophosphate, TFA = trifluoroacetic acid.

cedures were optimized by microwave activation to decrease the reaction times and improve conversion yields.

Preparation of key intermediate 6: Upon deprotection of the Fmoc group of the polystyrene AM RAM resin, the free amine group was acylated with bromoacetic acid in the presence of DIC (Scheme 2). A primary amine (first diversity source) was coupled to the bromo derivative to yield **4**, followed by treatment with allyl maleate in the presence of DIC and HOBt to obtain ester intermediate **5**. However, when the acylation reactions were assayed on substrates bearing an additional tertiary amino group, the conversion yields were much lower and complex mixtures profiles were obtained. In our experience, the use of this class of primary amine in a solid-phase synthesis of peptoids has resulted in the occurrence of problematic side reactions.[29] In these cases, the best results were obtained by using *O*-(benzotriazol-1-yl)-*N*,*N*,*N*,*N*-tetramethyluronium tetrafluoroborate (TBTU) and DIPEA to promote the reaction. Next, the second primary amine group was introduced by an aza-Michael reaction to render the intermediate ester **6**, which bears two of the three desired diversity sources. This reaction was the only one of the whole sequence that should be carried out at room temperature because nonreproducible results were obtained under microwave-assisted conditions. The NMR spectroscopic analysis of aliquot samples after their release from the resin showed that the addition of the amine group was regioselective and took place at the α-carbon atom to the amide group.

Preparation of 7-substituted perhydro-1,4-diazepine-2,5-dione derivatives 2: The secondary amine group of the intermediate ester **6** was acylated with bromoacetic acid and treated with the third primary amine to obtain **7**. The allyl ester group of **7** was removed. This deprotection could be conducted by treatment with $[Pd(PPh_3)_4]$ in the presence of $PhSiH_3$ in CH_2Cl_2. Alternatively, we observed that saponification could be performed by using 0.5 M KOH in dioxane (1:3) at room temperature or under microwave-assisted activation conditions. Finally, the solid-phase cyclization was promoted with PyBOP and HOBt in the presence of DIPEA to render final compound **2** after release from the resin using a TFA/CH_2Cl_2/H_2O mixture (see the Supporting Information for the synthetic details and characterization of **2a–f**). As anticipated, the use of a polymeric solid support provided a "pseudo-dilution effect" that favored the desired intramolecular cyclization.

Preparation of 3-substituted 1,4-piperazine-2,5-dione 3: In this case, the release of intermediate **6** from the resin afforded a crude reaction mixture, which under microwave conditions in dioxane, rendered the cyclized product **8** with quantitative conversion yields. Removal of the allyl moiety afforded the expected free carboxylic acid **9**. When an amine with an additional tertiary amino group was used in the first or second diversity position, the extraction of acid **9** into the organic phase was troublesome (20–30% yield). In this case, the hydrolysis of the ester was carried out in the solid phase followed by cleavage and cyclization as already described (see the Supporting Information for details of **3f**).

The crude reaction mixture containing free carboxylic acid **9** was used for coupling with the corresponding *N*-alkylglycinamide bearing the third diversity source. Initially, the amide formation was assayed in solution. To this aim, the previous synthesis of the *N*-alkylglycinamide by reaction of 2-chloroacetamide with the corresponding primary amine was attempted. Unfortunately, the results obtained were not satisfactory. The use of different solvents, reaction conditions, or reagent, that is, 2-bromoacetamide, resulted in incomplete conversion of the haloacetamide and, more importantly for the further purification process, the concomitant generation of dialkylation products. Therefore, we turned to a solid-phase preparation of the desired *N*-alkylglycinamides following the procedure developed for intermediate **4**. The reaction of crude compound **9** with selected *N*-alkylglycinamides was assayed. First, the *N*-alkylglycinamides were released and the amide formation was performed in solution; however, the results obtained were not satisfactory in terms of conversion yield. Therefore, the amide formation was carried out by linking the *N*-alkylglycinamide to the resin with DIC and HOBt as coupling agents. By using this procedure, title compounds **3a–e** were isolated in 30–40% overall yield after release from the resin. The only exception was the case of the 1,4-piperazine-2,5-dione **3f** in which TBTU and DIPEA should be employed as coupling agents for the final amide formation (see the Supporting Information for synthetic details and characterization for compounds **3a–f**).

Constriction by the formation of a heterocycle in **2** and **3** also produces a stereogenic center. The enantiopure compounds **2a** and **3a** were synthesized and characterized; however, we believe that the description of the enantiopure derivatives is beyond the scope of this study and will be reported elsewhere because the chirality of these compounds does not affect the present conformational study.

Structure of the conformationally constrained peptidomimetics 2 and 3 in solution: The knowledge of the conformation of **2** and **3** in solution is extremely important in understanding their biological activity and for the future redesign and optimization of a next generation of inhibitors. Therefore, we performed a conformational study by using NMR spectroscopic analysis and molecular modeling to understand both the thermodynamics and the kinetics of structures of **2** and **3** in solution. We selected **2a** and **3a** (Scheme 3) as initial compounds to study for several reasons. First, they displayed the less overlapping in the ^{1}H NMR spectra among the two families of peptidomimetics. Second, both molecules have shown interesting biological properties as inhibitors of the formation of the apoptosome.[21,27a]

The main feature in the ^{1}H and ^{13}C NMR spectra of **2a** and **3a** was the presence of two species in solution (in $CDCl_3$, CD_3CN, or deuterated dimethyl sulfoxide ([D_6]DMSO)), which interconvert slowly on the NMR time-

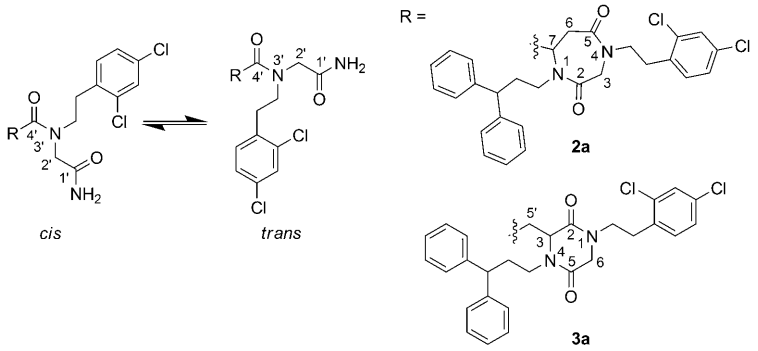

Scheme 3. Dynamic process responsible for the conformational behavior of **2a** and **3a** (an arbitrary numbering of the atoms has been adopted).

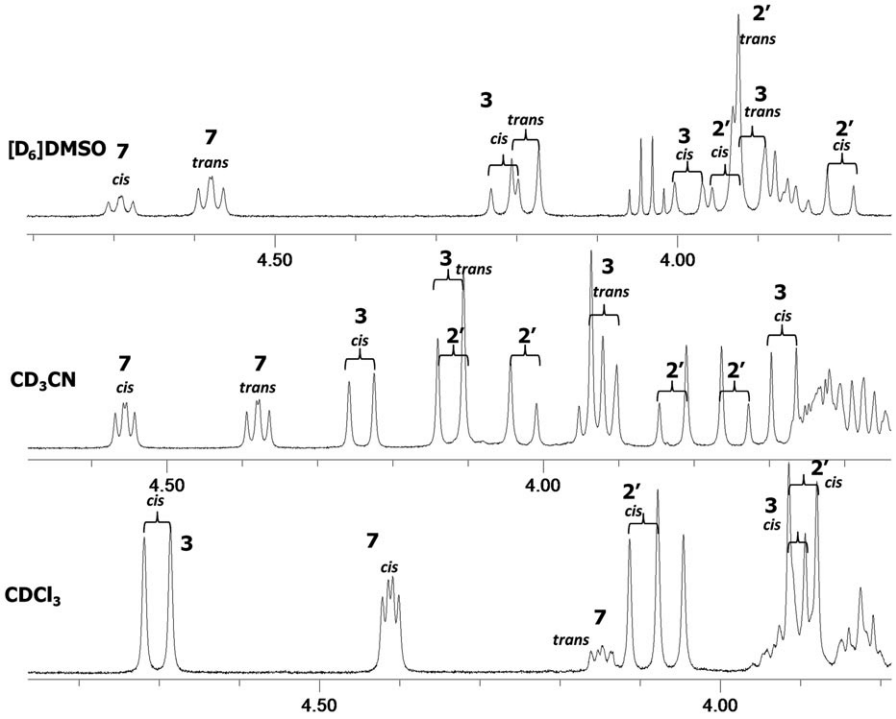

Figure 1. ^{1}H NMR spectra of **2a** in [D_6]DMSO, CD_3CN, and $CDCl_3$ (500 MHz, 303 K; see Scheme 3 for numbering).

scale (as observed at 300, 400, or 500 MHz). This fact was evident by the splitting of most of the ^{1}H and ^{13}C NMR peaks (see Figure 1 and the Supporting Information) for the corresponding proton signals interconnected by exchange processes (EXSY). For example, **2a** showed two different signals for the H7 proton of the chiral center of the molecule, which yielded negative cross peaks between them in the 2D ROESY spectra both in $CDCl_3$ and [D_6]DMSO (see the Supporting Information). Additionally, the dynamic nature of **2a**,**b** and **3a**,**b** has been further demonstrated by variable-temperature (VT) NMR experiments (see below). By considering previous studies on peptoids and the identity of the ^{1}H NMR signals that were split more significantly,[16] we proposed the *cis*/*trans* isomerization around the exocyclic tertiary amide bond to be the dynamic process responsible for this conformational behavior (Scheme 3).

Thermodynamic parameters: The unambiguous assignation of the NMR signals that correspond to each rotamer of **2a** and **3a** was accomplished by conclusive evidence (i.e., NOE interactions and chemical-shift differences). For example, in the case of **2a**, strong ROESY cross peaks were observed between $H6_{eq}$ and H2′ for the major isomer in $CDCl_3$, thus suggesting spatial proximity between the seven-membered ring and the methylene group of the terminal glycine unit (Scheme 4). This outcome implies that the major species in $CDCl_3$ must be the *cis* rotamer. On the other hand, the ROESY spectrum showed different correlations for the major isomer in [D_6]DMSO. The methylene group in the 2,4-dichlorophenethyl moiety directly attached to the nitrogen atom of the exocyclic amide group showed cross peaks with both the seven-membered-ring moiety and the methylene group of the terminal glycine unit, thus implying a preferred *trans* configuration in this solvent (Scheme 4).

These assignations are also consistent with the observed chemical-shift differences between both rotamers. Thus, the *trans* species (minor in $CDCl_3$, but major in [D_6]DMSO) would set the aromatic ring of the 2,4-dichlorophenethyl group attached to the exocyclic amide unit close to the H7 proton, thus explaining the observed lower chemical shift of this signal in this conformer (Figure 1). Although with a slightly larger overlapping of the ^{1}H NMR signals, a closely similar behavior was found for the six-membered-ring derivative **3a**. Likewise, the *cis* and *trans* isomers of **2b** and **3b** were assigned by chemical correlation and careful comparison of the corresponding NMR spectra. Integration of several proton bands rendered the corresponding population of the species, which were used to calculate the *cis*/*trans* equilibrium constants in different solvents (Table 1).

Comparison of the data in Table 1 shows that *cis* isomers are more favored in nonpolar environments, and that this preference is higher for the six-membered ring derivatives **3a**,**b**. When the polarity of the medium was increased, the

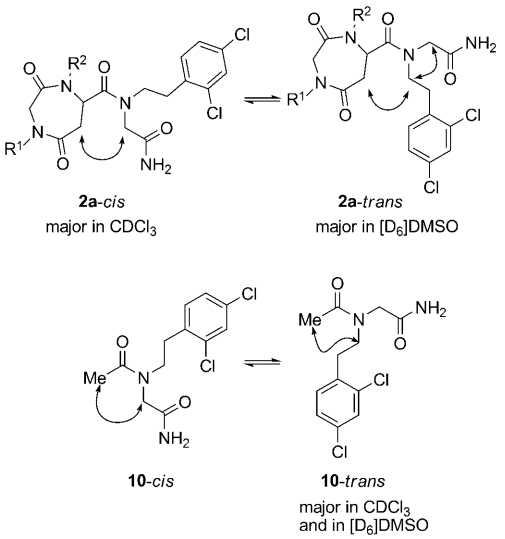

Scheme 4. Observed NOE interactions for the assignation of the *cis*/*trans* isomers for **2a** and **10**.

Table 1. Populations of the *cis*/*trans* isomers (*P*), estimated *cis*/*trans* equilibrium constants (K_{eq}), and Gibbs free energies ($\Delta G°$) for **2a**,**b** and **3a**,**b** at 303 K in different solvents.

Compound	Solvent	P_{cis} [%]	P_{trans} [%]	K_{eq} (*cis*→*trans*)	$\Delta G°$ (*cis*→*trans*) [kcal mol^{-1}]
2a	$CDCl_3$	77.0	23.0	0.30	0.72
	CD_3CN	50.0	50.0	1.00	0.00
	[D_6]DMSO	32.6	67.4	2.07	−0.44
2b	$CDCl_3$	77.0	23.0	0.30	0.72
	CD_3CN	46.1	53.9	1.17	−0.09
	[D_6]DMSO	30.4	69.6	2.29	−0.50
3a	$CDCl_3$	83.2	16.8	0.20	0.97
	CD_3CN	58.9	41.1	0.70	0.21
	[D_6]DMSO	50.0	50.0	1.00	0.00
3b	$CDCl_3$	82.3	17.7	0.21	0.92
	CD_3CN	54.1	45.9	0.85	0.10
	[D_6]DMSO	47.9	52.1	1.09	−0.05
10	$CDCl_3$	17.2	82.8	4.81	−0.92
	CD_3CN	38.4	61.6	1.60	−0.28
	[D_6]DMSO	46.3	53.7	1.16	−0.09

amount of *trans* isomer also increased. These data suggested that some intramolecular hydrogen-bonding interactions could play an important role in the *cis*/*trans* equilibrium process. To obtain deeper insight into this topic, model peptoid **10** was prepared and analyzed because this molecule represents an isolated version of the tertiary amide bond under study (Scheme 4). The assignations of the corresponding signals of the *cis*/*trans* isomers of **10** were done by 1D NOESY experiments (see the double-headed arrows in Scheme 4). Interestingly, for this compound, the *trans* configuration was favored in [D_6]DMSO, CD_3CN, and $CDCl_3$ (54, 62, and 83%, respectively). This observation suggested that the population increase of the *cis* isomer in the full-length molecules (i.e., **2a**,**b** and **3a**,**b**) was induced by the presence of the heterocyclic moiety.

By considering the molecular structure of the studied compounds, different intramolecular hydrogen-bonding patterns could be established (Figure 2a). For **2a**,**b** and **3a**,**b**, the *trans* isomers can establish intramolecular hydrogen bonds between the terminal amide NH group and one of the heterocyclic carbonyl groups, thus leading to the formation of either seven- or ten-membered rings, respectively. On the contrary, the *cis* isomers of the same molecules can only form the corresponding ten-membered rings because the seven-membered ring is geometrically impossible.[30] Finally, the simpler compound **10**, in which the ten-membered ring possibility was ruled out, can establish a seven-membered-ring hydrogen-bonding interaction in the *trans* isomer exclusively.

By taking into account these facts and the data shown in Table 1, we concluded that the seven-membered-ring hydrogen-bonding interaction stabilizes the *trans* configuration in **10**, although the *trans* isomer is also slightly preferred in the absence of this intramolecular hydrogen-bonding interaction (as it is expected to be the case in pure DMSO). The scenario is clearly more complicated with **2** and **3** because different hydrogen-bonding patterns can coexist. Theoretical calculations on simplified analogues of **2** and **3** suggested that the hydrogen bonding of the ten-membered ring is more favored than the seven-membered ring for the *trans* isomer, but there is practically no energetic difference between the *cis* and *trans* amide isomers in the ten-membered-ring hydrogen-bonded geometries (Figure 2b).

Compound **2a** yielded crystals suitable for X-ray diffraction analysis by very slow evaporation of a solution of the peptidomimetic in acetonitrile. Contrary to observations in solution at room temperature, only the *trans* isomer is present in the solid state. The intramolecular hydrogen bond HN-H···O=C(diazepine) partially fixes the conformation, thus closing a ten-membered ring (Figure 3, Table 2). Moreover, in the solid state, a centrosymmetric heterochiral dimer is formed as a result of the presence of two intermolecular HN-H···O=C-NH_2 hydrogen bonds (Figure 3, Table 2). These observations support the preference for the ten-membered ring in the *trans* isomer. We believe that the intermolecular hydrogen bonding in the crystal structure could be comparable to the effect of DMSO molecules in solution, thus providing a reasonable explanation for the preference of this rotamer both in the solid state and in polar environments. Taken all together, we found a good agreement between the behavior in solution, crystal structure, and theoretical results.

To shed additional light onto the behavior in solution, ^{1}H NMR titrations of solutions of **10**, **3a**, and **2a** in $CDCl_3$ with increasing amounts of [D_6]DMSO were performed

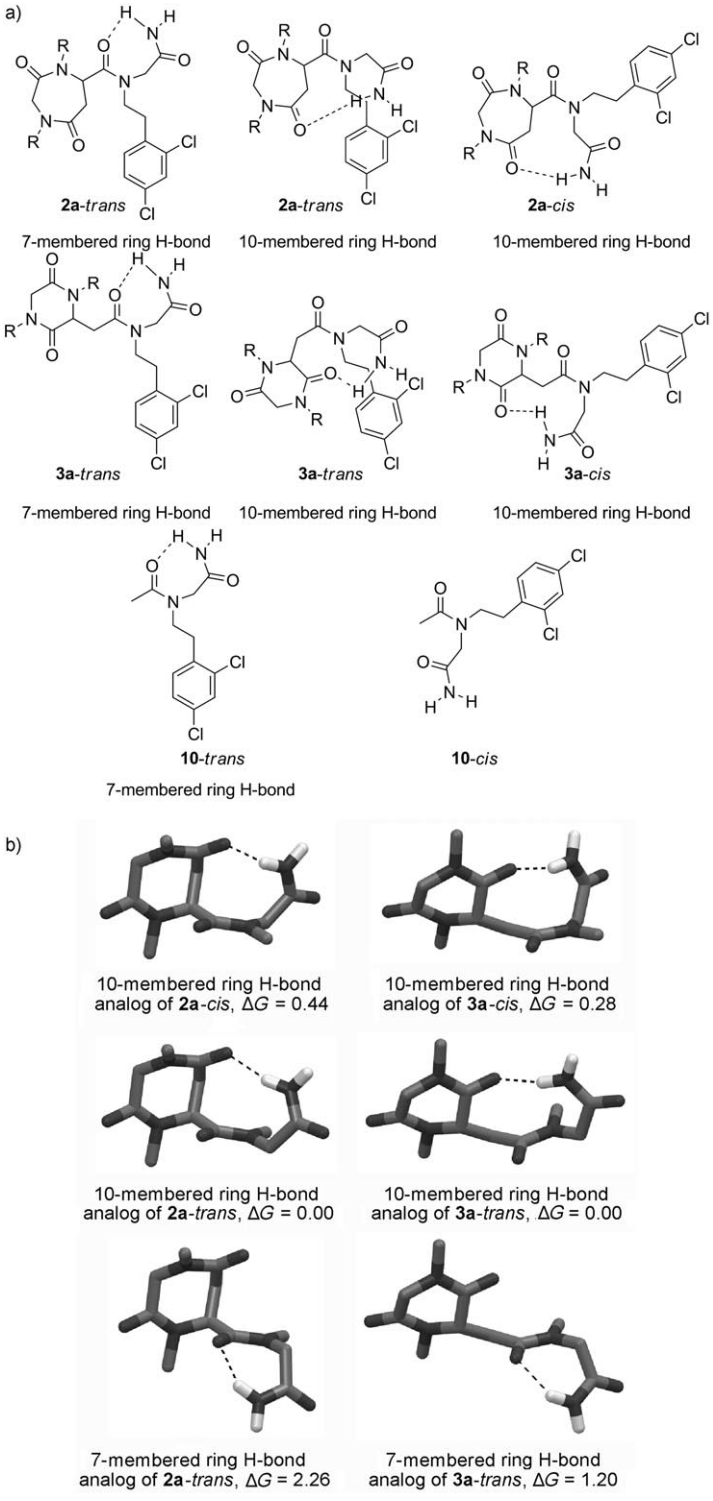

Figure 2. a) Schematic representation of the possible hydrogen-bonding patterns for **2a**, **3a**, and **10**. b) Optimized geometries and gas-phase ΔG values (kcal mol^{-1}) calculated at the B3LYP/6-31G** level for the hydrogen-bonded 10- and 7-membered rings of the *cis* and *trans* rotamers of simplified analogues of **2a** and **3a** in which the substituents R^1–R^3 have been replaced by methyl groups.

(Figure 4). Variations in the chemical shifts for the amide NH signals versus the amount of added DMSO were plotted for every isomer, whereas the population of the *cis* and *trans* isomers at every titration point were evaluated by the integration of the corresponding ^{1}H NMR signals. In this way, it was possible to monitor how the intramolecular hydrogen-bonding pattern was gradually broken by the action of DMSO and to evaluate the influence of this solvent on the *cis*/*trans* conformational equilibrium. An interesting behavior was observed in every case. For the simpler compound **10**, the *cis* isomer shows a large dependence of the chemical shifts for the NH signal on added DMSO, as expected for a non-hydrogen-bonded amide proton. On the contrary, the NH protons in the *trans* isomer are less accessible to the solvent (i.e., DMSO) as a result of the occurrence of an intramolecular hydrogen bond, which is reflected in a lower dependence of the chemical shifts for the NH signal on the addition of DMSO. Concomitantly, when the proportion of DMSO increases, the percentage of the *cis* isomer also increases, although the *trans* isomer is always more stable in this model system. These experiments are in accordance with our initial proposal on the effect of the hydrogen-bonding interactions on the *cis*/*trans* equilibrium of **10**. On the other hand, the *trans* isomer for **3a** showed a larger dependence of the chemical shifts for the NH signal on the added DMSO, thus suggesting that the possible hydrogen-bonding pattern is less favored by this rotamer. In this case, the NH protons in the *cis* isomer are less accessible to the solvent (i.e., DMSO) as shown by the lower dependence of the chemical shifts for the NH signal. When the proportion of DMSO increases, the amount of *trans* isomer also increases, thus suggesting that the intermolecular hydrogen bonding stabilizes the *trans* isomer, whereas the intramolecular hydrogen bonding stabilizes the *cis* isomer.

Only one NH proton could be monitored for every rotamer of **2a**, but the trends were similar to those observed for **3a**. However, other structurally interesting parameters were observable as a result of decreased signal overlapping in the aliphatic proton region. The coupling constants of H7/H6 in the *cis* rotamer ($^3J_{H7,H6_{eq}} = 3.7$ and $^3J_{H7,H6_{ax}} = 6.3$ Hz) and the large anisochrony of the methylene protons at C6, C3, and C2′ ($\Delta\delta = 0.234$, 1.159, and 0.199 ppm, respectively) in pure $CDCl_3$ support the presence of a conformation rigidified by an intramolecular hydrogen bond. As previously mentioned, this behavior has to be through a ten-membered ring. When adding DMSO, the amount of *trans* isomer increased and, for this rotamer, the anisochrony of the diastereotopic protons H3 and H6 is lower, in the same way as those for the terminal glycine H2′. In addition, the corresponding coupling constants between H7 and $H6_{ax}$/$H6_{eq}$ are similar, which are the consequence of breaking the intramolecular hydrogen-bonded ten-membered ring to give a more flexible structure in solution. All these data support the fundamental roles that the polarity of the medium and the intramolecular hydrogen-bonding pattern play in the *cis*/*trans* conformational equilibrium of these peptidomimetics. The intramolecularly hydrogen-bonded ten-membered ring (only possible with **2a** and **3a**) favors the *cis* isomer in nonpolar environments. As this hydrogen-bonding interaction is gradually

Table 2. Geometries of the main hydrogen bonds in the crystal structure of **2a** (see Figure 3).[a]

Hydrogen-bond lengths [Å]		Hydrogen-bond angles [°]	Hydrogen-bond type
N22···O2	H22B···O2	N22−H22B···O2	intra
2.945(4)	2.18	149	
N22···N21	H22B···N21	N22−H22B···N21	intra
2.835(4)	2.46	107	
		O2···H22B···N21	
		102	
N22···O22	H22A···O22	N22-H22A···O22	inter
3.040(4)	2.21	161	

[a] Distances N22−H22A and N22−H22B are fixed at 0.86 Å.

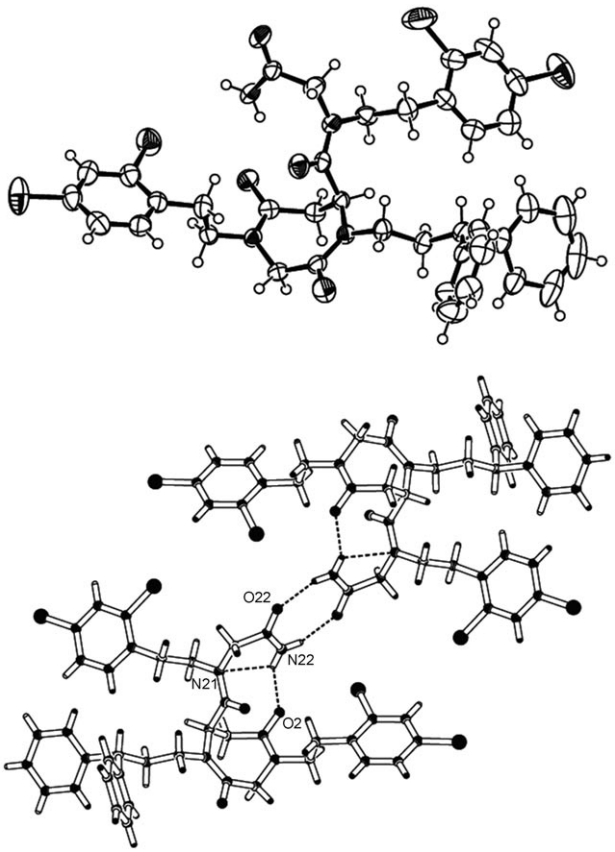

Figure 3. Molecular structure of **2a** in the solid state (up, ellipsoid plot with 50% probability) and dimer of **2a** in the crystal structure (down, dashed lines represent hydrogen bonds).

broken by increasing the polarity of the medium, the corresponding proportion of the *trans* rotamers increases. Furthermore, the proposed ten-membered rings would be less strained in **3a**,**b** than in **2a**,**b**, thus explaining the slightly higher population of the *cis* isomers in the 1,4-piperazine-2,5-dione family.

Kinetic parameters: Once the thermodynamic parameters of the *cis*/*trans* equilibria for the representative peptidomimetics **2a**,**b** and **3a**,**b** were characterized, we also attempted to study the kinetics of the interconversion. With this aim, VT-NMR spectroscopic experiments were performed in [D_6]DMSO for both derivatives. This solvent allowed higher temperatures to be reached and also minimized the intramolecular hydrogen-bonding effects. A severe broadening of the ^{1}H NMR spectra was obtained upon heating (see the Supporting Information), thus leading to the coalescence of several signals and allowing the energetic barrier for the amide rotation to be estimated (Table 3). As **2a** exists in unequal populations of *cis* and *trans* rotamers in DMSO, the corresponding energetic barriers were calculated as described by Shanan-Atidi and Bar-Eli.[31] The simplified formula for isoenergetic species was applied for **3a**.[32] For both compounds, several proton signals could be used as probes and showed a good internal consistency within the estimated error for these approximated formulae (± 0.4 kcal mol^{-1}). The energetic barriers are in the range of 19–20 kcal mol^{-1}, which is in good agreement with those previously reported for similar systems.[16] A slightly lower interconversion barrier was obtained for the six-membered-ring derivative, although the difference is close to the experimental error by using the corresponding approximated formulae at the coalescence temperature. As the coalescence of different signals of a given compound occurred at different temperatures, we roughly estimated a small effect of temperature on the energetic barrier. Therefore, there must be a small entropic contribution to $\Delta G^{\neq}$, as expected for a dynamic process based on the rotation of a single C−C bond.

Unfortunately, attempts to perform the full line-shape analysis of the VT-NMR experiments for **2a**,**b** and **3a**,**b** were unsatisfactory as a result of the complex spin systems implicated and the severe signal overlapping. Therefore, the entropic and enthalpic contributions to the activation parameters could not be obtained accurately. As the rotational barrier did not seem to be significantly affected by the substitution on the tertiary amide bond (R in Scheme 3), we decided to perform VT-NMR spectroscopic experiments with the simpler peptidomimetic model **10** bearing a methyl group instead of the heterocyclic scaffold. In this case, the dynamic process was isolated and could be studied more precisely. VT-NMR spectroscopic experiments in DMSO produced the coalescence of four signals, which are the associated energy barriers summarized in Table 3. The results obtained are in reasonable agreement with those previously found ($\Delta G^{\neq} \approx 19$ kcal mol^{-1}). In this case, we could carry out the full line-shape analysis of the methyl signal within the temperature range 333–393 K (Figure 5). The accurate Eyring and Arrhenius plots yielded the corresponding activation parameters for the *cis*/*trans* isomerization in both directions of the equilibrium. The results demonstrate the negligible entropic contribution to the energetic barrier for this conformational process (Table 4). These data support our initial estimation for **2a** and **3a**, which are also in good agreement with results reported on related systems.[16]

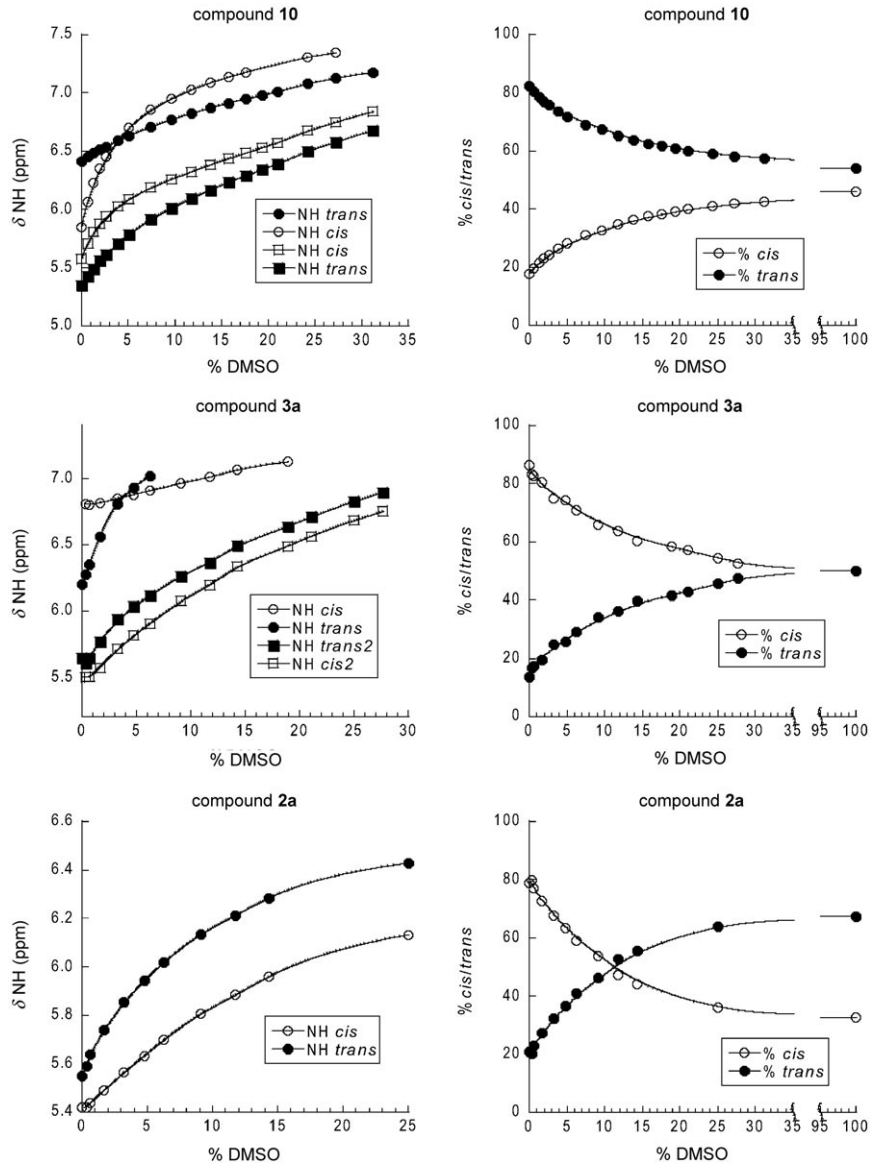

Figure 4. Plots of the chemical shifts for the amide NH signal (left) and proportions of the *cis*/*trans* isomers (right) of **10**, **3a**, and **2a** ($CDCl_3$, 303 K, 500 MHz) versus the percentage of [D_6]DMSO (*cis*/*trans* isomers are given as hollow and solid symbols, respectively).

The computational conformational analysis of **10** supported the above observations. The conformational space of **10** was systematically explored by molecular mechanics methods to find relevant energy minima. In this way, 68 different conformers with energies within 10 kcal mol^{-1} from the lowest-energy minimum were located and reoptimized by DFT methods at the B3LYP/6-31G** level (see the Supporting Information). The interconversion among different pairs of low-energy *cis*/*trans* amide conformers was studied and the corresponding transition states were determined (see the Supporting Information). Figure 6 shows the structures of the most-relevant energy minima and of the lowest-energy transition state detected in the gas phase, and Table 5 reports the geometric and energetic parameters for the same structures.[34]

Hence, the lowest free-energy conformer of **10** (*trans*-1) shows the expected hydrogen bond between the terminal amide NH_2 group and the carbonyl oxygen atom of the acetamide group, in accord with the NMR results. The hydrogen bond is maintained in the lowest energy transition state detected for the interconversion between *cis*/*trans* amide conformers (TS-1). The calculated free energy of TS-1 is 19.3 kcal mol^{-1}, in agreement with the experimental results obtained by NMR spectroscopic analysis. Transition state TS-1 is connected to conformers *trans*-3 and *cis*-3 by rotation of dihedral angle ω with concomitant rotation of dihedral angle χ_1 and pyramidalization of the planar amide nitrogen atom. The minimum energy conformer *trans*-3 is 1.17 kcal mol^{-1} above the lowest-energy *trans*-1 conformer, through which it is related by a low barrier rotation of the dihedral angles χ_1 and χ_3. Whereas the minimum *cis*-3 is 1.35 kcal mol^{-1} above the lowest-energy *cis* conformer (*cis*-1), with which it is connected again through a low barrier rotation around the dihedral angle χ_3.

Conclusion

The partial restriction of the conformational flexibility of peptoids by means of designing two families of peptidomimetics based on the perhydro-1,4-diazepine-2,5-dione **2** and the 1,4-piperazine-2,5-dione **3** scaffolds has been studied. To this end, we have developed a versatile (for diversity-oriented strategies), solid-phase synthesis of both families from a common intermediate **6** in good overall yield. The synthetic pathway involves the generation of **6** by a regioselective aza-Michael addition and the extensive use of microwave activation to decrease reaction times while maintaining purity and conversion yield of the different intermediates and final products.

From the conformational behavior of these peptidomimetic families, some conclusions can be drawn that are of importance for the study of the peptidomimetic/biological-target interactions and for further peptidomimetic structural

Table 3. Frequency difference ($\Delta\nu$), coalescence temperature (T_c), and energetic barrier at T_c ($\Delta G^{\&\#8225;}$) for the conformational process in peptidomimetics **2a**,**b**, **3a**,**b**, and **10**.

Compound	Signal	$\Delta\nu$ [Hz]	T_c [K]	$\Delta G^{\ddagger}$ (*cis*→*trans*)[a] [kcal mol^{-1}]	$\Delta G^{\ddagger}$ (*trans*→*cis*)[a] [kcal mol^{-1}]
2a	H7	31.5	388	19.6	20.1
	H3	7.5	363	19.3	19.8
	H3	8.1	363	19.2	19.8
	average[b]			19.4	19.9
2b	H7	36.6	388	19.4	20.0
	H3	5.2	355	19.1	19.6
	average[b]			19.3	19.8
3a	H3	10.5	363	19.1	–
	H6	6.2	341	19.2	–
	H6	18.2	373	19.2	–
	average[b]			19.2	–
3b	H6	18.0	371	19.1	–
10	H2′	13.5	360	18.7	18.9
	NCH_2	16.8	365	18.8	19.0
	CH_2Ar	32.4	373	18.7	19.0
	Me	8.1	363	19.2	19.5
	average[b]			18.9	19.1

[a] Estimated error: ±0.4 kcal mol^{-1}. [b] Average value using different proton signals.

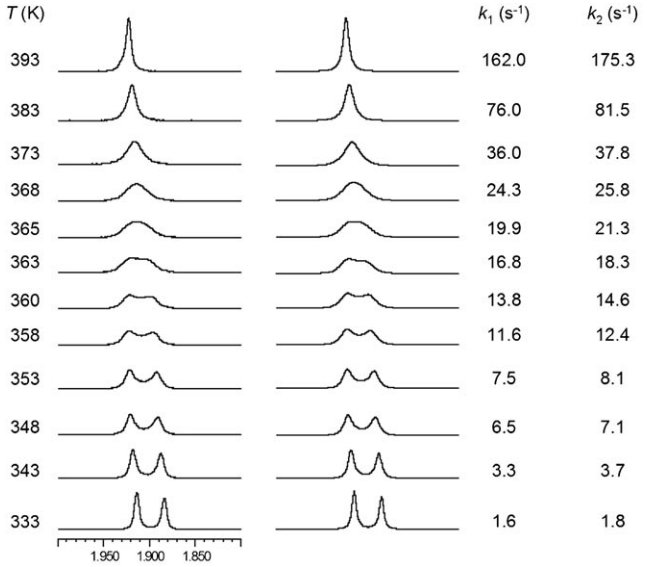

Figure 5. Experimental (left) and simulated (right) VT-NMR spectra of the methyl signal of **10** (300 MHz). Temperatures and computed exchange rates k are also given for every trace. The simulated spectra were obtained with the gNMR program.[33]

Table 4. Activation parameters for the methyl signal of **10**.

Activation parameters	*cis*→*trans*	*trans*→*cis*
$\Delta H^{\ddagger}$ [kcal mol^{-1}][a]	19.28	19.39
$\Delta S^{\ddagger}$ [cal (K mol)$^{-1}$][b]	0.1	0.2
$\Delta G^{\ddagger}_{298K}$ [kcal mol^{-1}][a]	19.28	19.32
E_a [kcal mol^{-1}][a]	19.96	20.07

[a] Estimated error: ±0.15 kcal mol^{-1}. [b] Estimated error: ±0.5 cal (K mol)$^{-1}$.

optimization toward more active compounds. First, the large population of *cis* amide isomers in these systems is rather remarkable. It has been recently reported that in peptoids the *trans* configurations prevail in solution, although important proportions of the *cis* rotamers are also present.[16] In addition, the *trans* (*cis*) configuration is favored even more when the other amide bonds have *trans* (*cis*) disposition. In our peptidomimetic systems, two amide bonds are frozen in a *cis* configuration as a result of the constraints of the corresponding cyclic structure. Accordingly, an increased proportion of the *cis* rotamer should be expected for the free exocyclic amide bond, which is exactly what we observed. More interestingly, we have demonstrated that the pro-

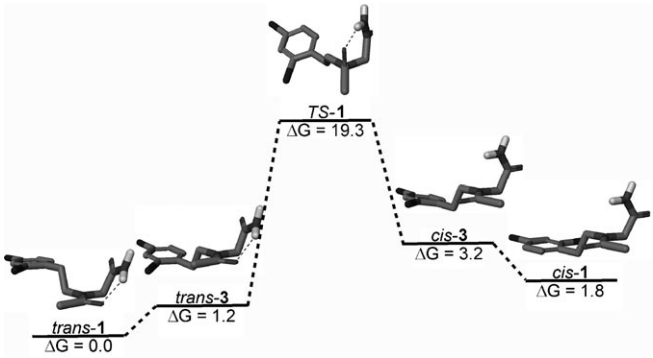

Figure 6. Relevant low-energy *cis* and *trans* amide conformers and the lowest-energy transition state determined at the B3LYP/6-31G** level for **10**. The numbering of the *cis*/*trans* conformers and transition states corresponds to increasing free energy (see the Supporting Information).

portion of *cis*/*trans* isomers is highly affected by the polarity of the solvent as a result of the possibility of establishing an intramolecular hydrogen-bonding pattern. Therefore, the population of the *cis*/*trans* isomers of the compounds studied herein under thermodynamic control could serve as a molecular probe for the polarity of the microenvironment that surrounds these molecules. This parameter could be used in ideal systems to map the polarity of binding pockets on targeted biomolecules. In addition, the kinetic parameters of the binding must be also carefully considered. Usually, the kinetics of the receptor/ligand interaction is fast on the NMR timescale.[35] On the other hand, our studies showed that the *cis*/*trans* isomerization of the amide bond is slow on the NMR timescale. Therefore, the binding phenomena must be faster than the amide-bond rotation and accordingly both rotamers would look like different molecules to the biomolecular receptor. Moreover, we should keep in mind that binding rates are concentration dependent but amide rotation is a unimolecular process. Therefore, knowledge of

Table 5. Geometries ({ω, ϕ, ψ, χ_1, χ_2, χ_3} and $d_{NH\cdots O}$), ΔE, and ΔG values determined in the gas phase for the conformations shown in Figure 6.

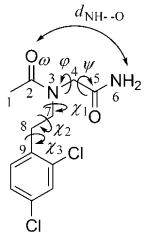

Conformer	ω [°]	ϕ [°]	ψ [°]	χ_1 [°]	χ_2 [°]	χ_3 [°]	$d_{NH\cdots O}$ [Å]	ΔE [kcal mol^{-1}]	ΔG [kcal mol^{-1}]
trans-**1**	−176.8	−83.5	79.3	96.0	173.6	81.7	2.03	0.79	0.00
trans-**3**	−178.5	−86.6	80.4	−103.8	−175.6	−85.4	2.09	2.00	1.17
cis-**1**	7.7	−98.9	5.6	−81.3	177.4	85.2	3.62	4.36	1.80
cis-**3**	6.7	−102.1	11.5	−83.8	−173.5	−82.9	3.61	5.70	3.15
TS-**1**	−109.2	−91.0	55.3	−163.5	−175.2	−84.4	1.99	20.7	19.3

the strength (and kinetics) of the interaction should be crucial for the selection of a suitable experimental technique and the optimal concentration range in carrying out biomolecular binding studies with these peptidomimetic systems.

Experimental Section

General: All the reagents were obtained from commercial sources and used without further purification. Polystyrene AM RAM resin (0.75 mmol g^{-1}) was purchased from Rapp Polymere GmbH (Germany). Polypropylene syringes fitted with a polyethylene disc were used for the reactions carried out in a HS501 Digital IKA Labortechnik stirrer. Microwave-assisted reactions were performed in a CEM Discover microwave reactor using a 10 mL glass reaction vessel. Coupling efficiencies were monitored using the 2,4,6-trinitrobenzenesulfonic acid (TNBS) test for primary amines, the chloranil test for secondary amines, and the malachite green test for carboxylic acids. Analytical reverse-phase (RP) HPLC was performed with a Hewlett Packard Series 1100 (UV detector 1315A) modular system on a reverse-phase Kromasil 100 C_8 column (15×0.46 cm, 5 μm) and a X-Terra C_{18} column (15×0.46 cm, 5 μm). Solvent mixtures of CH_3CN/H_2O containing 0.1% TFA at a flow rate of 1 mL min^{-1} were used as the mobile phase and the monitoring wavelength was set at $\lambda = 220$ nm. Semipreparative RP-HPLC was performed on a Waters system (Milford, MA, USA) on a X-Terra C_{18} column (19× 250 mm, 5 μm). High-resolution mass spectra (HRMS-FAB) were carried out at the Mass Spectrometry Service of the University of Santiago de Compostela (Spain) and at the IQAC Mass Spectrometry Service.

NMR spectroscopic analysis: The NMR samples were prepared at concentrations of 10 mM. The NMR spectroscopic experiments were carried out either on a Varian INOVA 500 spectrometer (500 and 125 MHz for ^{1}H and ^{13}C, respectively) or a Varian MERCURY 400 spectrometer (400 and 100 MHz for ^{1}H and ^{13}C, respectively). To take advantage of the magnetic field value, measurements that required temperatures higher than room temperature for observing coalescence were performed in an apparatus with a proton resonance frequency of 300 MHz (Varian UNITY 300 spectrometer). Bidimensional NMR spectroscopic experiments (gDQCOSY, gHSQC, gHMBC, ROESY, and 1D NOESY) were acquired by using the standard pulse sequences and parameter sets as found in VNMRJ. Chemical shifts δ are given in ppm relative to the internal reference trimethylsilane (TMS), and the coupling constants J are reported in Hertz (Hz).

X-ray crystallographic studies: Crystals of **2a** were grown from a concentrated solution in acetonitrile. One crystal was mounted on a glass fiber, and measurements were made with a Bruker SMART-APEX CCD area-detector diffractometer at room temperature with graphite-monochomatized MoKα radiation. Lorentz polarization and absorption corrections were applied using Bruker SAINT[36] and SADABS[37] software. The structure was solved by direct methods and refined by full-matrix least squares on $F2$ for all unique measured data using SHELXTL.[38] Non-hydrogen atoms were refined anisotropically. Hydrogen atoms were included with riding-model constraints and isotropic displacement parameters equal to 1.2 times the U_{eq} values of the corresponding carbon or nitrogen atoms. The following crystal structure has been deposited at the Cambridge Crystallographic Data Centre and allocated the deposition number CCDC 808273.

Computational methods: Molecular mechanics (MM) calculations were performed with the program MOE 2007.09 (Chemical Computing Group, Montreal, Canada) and quantum-mechanics calculations with the program Jaguar 7.5.[39] The MMFF94x force field, a modified version of the MMFF94s force field[40] implemented in the MOE program, was used for all MM energy calculations by using distance-dependent electrostatics ($\varepsilon = 1$) without cut-off points to model the nonbonded interactions. The systematic conformational search method implemented in the same program was used to determine the minimum energy conformations on the potential-energy hypersurface of **10**. For this purpose, the dihedral angles ω, ϕ, ψ, χ_1, χ_2, and χ_3 were varied systematically with angle steps of 180, 120, 60, 120, 120, and 60°, respectively. The generated conformations were then minimized and, after removing duplicate and isoenergetic symmetry-related conformations (those with dihedral angles {ω, ϕ, ψ, χ_1, χ_2, χ_3} and {$-\omega$, $-\phi$, $-\psi$, $-\chi_1$, $-\chi_2$, $-\chi_3$}), all the resulting minima within 10 kcal from the lowest-energy minimum were used as starting points for subsequent geometry optimizations by using quantum mechanical methods. All the minima were optimized at the B3LYP/6–31G** level of theory, that is, by using the hybrid of the Becke three-parameter exchange functional (B3)[41] combined with the Lee, Yang, and Parr (LYP) exchange-correlation functional[42] and the 6–31G** basis set. Transition states for the interconversion between selected low-energy *cis*/*trans* pairs of conformers were determined at the same level of theory. For this purpose, four possible transition-state structures for each *cis*/*trans* pair were considered. These four structures arise from two possible directions, namely, clockwise and counterclockwise, for the twist of the amide bond and concomitant pyramidalization of the amide nitrogen atom above or below the plane of the amide group.[43] Frequency analyses were carried out to characterize the nature of the determined stationary points as either minima (no imaginary frequency) or transition states (single imaginary frequency) and to calculate the zero-point vibrational energies and the thermal and entropic corrections from which the conformational free energies in the gas phase were determined.

Synthesis of perhydro-1,4-diazepine-2,5-dione derivatives 2 (Scheme 2): The synthesis of these compounds was carried out by using a general procedure on a 1% cross-linked polysterene resin bearing the Fmoc-protected Rink amide linker AM RAM (0.75 mmol g^{-1}). The resin was filtered and washed with DMF (3×4 mL), *i*PrOH (3×4 mL), and CH_2Cl_2 (3× 4 mL) after each reaction. The ten-step synthesis proceeded as follows:

1) Removal of the Fmoc group: The Rink amide resin was treated with a solution of piperidine in DMF (20%) and the reaction mixture was stirred under microwave activation for 2 min at 60°C.

2) Acylation with bromoacetic acid: The resin was treated with a solution of bromoacetic acid (5 equiv) and DIC (5 equiv) in DMF. The reaction mixture was stirred under microwave activation for 1 min at 35°C. The resin was drained and washed.

3) Amine coupling: A solution of appropriate primary amine (5 equiv) and triethylamine (5 equiv) in DMF was added to the resin and the suspension was stirred for 2 min at 90 °C under microwave activation. The supernatant was removed, and the residue was drained and washed.

4) Acylation with allyl maleate: The resin was treated with a solution of allyl maleate (5 equiv), HOBt (5 equiv), and DIC (5 equiv) in CH_2Cl_2/DMF (2:1). The reaction mixture was stirred under microwave activation for 1 min at 45 °C and filtered.

5) Michael addition: A solution of the corresponding primary amine (5 equiv) and triethylamine (5 equiv) in DMF (4 mL) was added to the resin and the suspension was stirred for 16 h at 20 °C. The supernatant was removed, and the residue was drained and washed.

6) Acylation with bromoacetic acid: The resin was treated as described in step 2.

7) Amine coupling: The resin was treated as described in step 3.

8) Removal of the allyl ester: The resin was treated with 0.5 M KOH (5 equiv) in dioxane for 4 min at 110 °C under microwave activation. The supernatant was removed and the residue was drained and washed.

9) Cyclization on a solid phase: The intramolecular cyclization was promoted by treatment with PyBOP (1.5 equiv), HOBt (1.5 equiv), and DIPEA (3 equiv) in DMF (4 mL). The mixture was stirred for 20 min at 60 °C under microwave activation and filtered. The solvent was removed by filtration and the resin was washed. The cyclization was checked by testing with chloranil, and if necessary the process was repeated under the same conditions.

10) Cleavage of the resin: The resin was treated with a mixture of TFA/CH_2Cl_2/H_2O (60:40:2, v/v/v) for 30 min at room temperature. The cleavage mixture was filtered and the solvent was removed under reduced pressure. The residue obtained was purified by semipreparative RP-HPLC with the appropriate CH_3CN/H_2O gradient.

Synthesis of 3-substituted 1,4-piperazine-2,5-dione derivatives 3 (Scheme 2): The synthesis of these compounds was carried out by using a general procedure on the resin described above. Unless stated otherwise, the reaction time and further treatment of the crude reaction mixtures were analogous to those described above for the synthesis of **2**. The resin was filtered and washed with DMF (3×4 mL), *i*PrOH (3×4 mL), and CH_2Cl_2 (3×4 mL) after each reaction. First, the Rink amide resin was treated as described above in steps 1–5.

6) Cleavage of the resin: The resin was treated with a mixture of TFA/CH_2Cl_2/H_2O (60:40:2, v/v/v) for 30 min at room temperature. The cleavage mixture was filtered and the solvent was removed by evaporation under reduced pressure. Traces of water and acid were removed by washing with CH_3CN (3×5 mL), which was also removed under reduced pressure.

7) Cyclization in solution to obtain intermediate **8**: Cyclization was promoted by treating the cleavage mixture with dioxane for 4 min at 120 °C under microwave conditions (HPLC monitoring).

8) Removal of the allyl ester in solution: A solution of 4 M NaOH and allyl alcohol (1:2 v/v) was added to intermediate **8** in dioxane (1:4) and the mixture was stirred for 4 min at 90 °C under microwave activation (monitoring by HPLC). The crude reaction mixture was acidified with 1 M HCl and the organic solvent was evaporated. The resulting residue was extracted with EtOAc, dried over anhydrous $MgSO_4$, and concentrated in vacuo.

The removal of the allyl ester to obtain **9e** was carried out on a solid phase under the conditions described previously to obtain **2**. After cleavage of the resin with a solution of TFA/CH_2Cl_2/H_2O (60:40:2 v/v/v) for 30 min at room temperature, the residue obtained from the evaporation of the crude reaction mixture was treated with dioxane for 30 min under reflux.

9) Amide formation: The different peptoidyl resins **4** were synthesized as described above in steps 1–3. The corresponding intermediate **9** (0.25 mmol) was coupled onto the resin containing the *N*-alkylglycine residue (1 equiv) in the presence of HOBt (0.4 mmol) and DIC (0.4 mmol) in CH_2Cl_2/DMF (1:1). In the case of **3e**, the mixture PyBOP (0.4 mmol) and DIPEA (0.8 mmol) in DMF was used as the coupling agent. The reaction mixtures were stirred for 3 h at room temperature and filtered. The resin was drained and washed.

10) Cleavage of the resin: Treatment of the resin as described above afforded a crude reaction mixture containing the title compound **3**, which was purified by semipreparative RP-HPLC with the appropriate CH_3CN/H_2O gradient.

Acknowledgements

Support from MICINN (Grants CTQ2005-00995, SAF2008-00048, BIO2007 60066) is acknowledged. The authors thank F. J. Morales and M. Camargo for technical assistance. A JAE-CSIC fellowship to A.M. is also acknowledged.

[1] R. J. Simon, R. S. Kania, R. N. Zuckermann, V. D. Huebner, D. A. Jewell, S. Banville, S. Ng, L. Wang, S. Rosenberg, C. K. Marlowe, D. C. Spellmeyer, R. Tan, A. D. Frankel, D. V. Santi, F. E. Cohen, P. A. Bartlett, *Proc. Natl. Acad. Sci. USA* **1992**, *89*, 9367–9371.

[2] a) G. M. Figliozzi, R. Goldsmith, S. C. Ng, S. C. Banville, R. N. Zuckermann, N. A. John, *Methods Enzymol.* **1996**, *267*, 437–447; b) H. J. Olivos, P. G. Alluri, M. M. Reddy, D. Salony, T. Kodadek, *Org. Lett.* **2002**, *4*, 4057; c) B. C. Gorske, S. A. Jewell, E. J. Guerard, H. E. Blackwell, *Org. Lett.* **2005**, *7*, 1521–1524.

[3] R. N. Zuckermann, J. M. Kerr, S. B. H. Kent, W. H. Moos, *J. Am. Chem. Soc.* **1992**, *114*, 10646–10647.

[4] S. M. Miller, R. J. Simon, S. Ng, R. N. Zuckermann, J. M. Kerr, W. H. Moos, *Bioorg. Med. Chem. Lett.* **1994**, *4*, 2657–2662.

[5] R. N. Zuckermann, E. J. Martin, D. C. Spellmeyer, G. B. Stauber, K. R. Shoemaker, J. M. Kerr, G. M. Figliozzi, D. A. Goff, M. A. Siani, R. J. Simon, S. C. Banville, E. G. Brown, L. Wang, L. S. Richter, W. H. Moos, *J. Med. Chem.* **1994**, *37*, 2678–2685.

[6] T. M. Ross, R. N. Zuckermann, C. Reinhard, W. H. Frey II, *Neurosci. Lett.* **2008**, *439*, 30–33.

[7] J. T. Nguyen, M. Porter, M. Amoui, W. T. Miller, R. N. Zuckermann, W. A. Lim, *Chem. Biol.* **2000**, *7*, 463–473.

[8] T. Hara, S. R. Durell, M. C. Myers, D. H. Appella, *J. Am. Chem. Soc.* **2006**, *128*, 1995–2004.

[9] P. Mora, I. Masip, N. Cortés, R. Marquina, R. Merino, J. Merino, T. Carbonell, I. Mingarro, A. Messeguer, E. Pérez-Payá, *J. Med. Chem.* **2005**, *48*, 1265–1268.

[10] J. A. Patch, A. E. Barron, *J. Am. Chem. Soc.* **2003**, *125*, 12092–12093.

[11] C. Garcia-Martinez, M. Humet, R. Planells-Cases, A. Gomis, M. Caprini, F. Viana, E. De La Pena, F. Sanchez-Baeza, T. Carbonell, C. De Felipe, E. Perez-Paya, C. Belmonte, A. Messeguer, A. Ferrer-Montiel, *Proc. Natl. Acad. Sci. USA* **2002**, *99*, 2374–2379.

[12] C. W. Wu, S. L. Seurynck, K. Y. C. Lee, A. E. Barron, *Chem. Biol.* **2003**, *10*, 1057–1063.

[13] P. A. Wender, D. J. Mitchell, K. Pattabiraman, E. T. Pelkey, L. Steinman, J. B. Rothbard, *Proc. Natl. Acad. Sci. USA* **2000**, *97*, 13003–13008.

[14] K. Kirshenbaum, A. E. Barron, R. A. Goldsmith, P. Armand, E. K. Bradley, K. T. V. Truong, K. A. Dill, F. E. Cohen, R. N. Zuckermann, *Proc. Natl. Acad. Sci. USA* **1998**, *95*, 4303–4308.

[15] a) M. Kuemin, Y. A. Nagel, S. Schweizer, F. W. Monnard, C. Ochsenfeld, H. Wennemers, *Angew. Chem.* **2010**, *122*, 6468–6471; *Angew. Chem. Int. Ed.* **2010**, *49*, 6324–6327; b) W. J. Wedemeyer, E. Welker, H. A. Scheraga, *Biochemistry* **2002**, *41*, 14637–14644.

[16] The *cis*/*trans* conformers of the tertiary amide bond in peptoids were named following the nomenclature in this field; for example, see: Q. Sui, D. Borchardt, D. L. Rabenstein, *J. Am. Chem. Soc.* **2007**, *129*, 12042–12048.

[17] a) B. C. Gorske, B. L. Bastian, G. D. Geske, H. E. Blackwell, *J. Am. Chem. Soc.* **2007**, *129*, 8928–8929; b) S. A. Fowler, H. E. Blackwell, *Org. Biomol. Chem.* **2009**, *7*, 1508–1524.

[18] a) J. A. Patch, A. E. Barron, *Curr. Opin. Chem. Biol.* **2002**, *6*, 872–877; b) R. C. Elgersma, G. E. Mulder, J. A. W. Kruijtzer, G. Posthuma, D. T. S. Rijkers, R. M. J. Liskamp, *Bioorg. Med. Chem. Lett.* **2007**, *17*, 1837–1842.

[19] E. Pérez-Payá, M. Orzáez, L. Mondragón, D. Wolan, J. A. Wells, A. Messeguer, M. J. Vicent, *Med. Res. Rev.* **2010**, DOI: 10.1002/med.20198.

[20] I. Masip, N. Cortes, M. J. Abad, M. Guardiola, E. Perez-Paya, J. Ferragut, A. Ferrer-Montiel, A. Messeguer, *Bioorg. Med. Chem.* **2005**, *13*, 1923–1929.

[21] G. Malet, A. G. Martin, M. Orzáez, M. J. Vicent, I. Masip, G. Sanclimens, A. Ferrer-Montiel, I. Mingarro, A. Messeguer, H. O. Fearnhead, E. Pérez-Payá, *Cell Death Differ.* **2006**, *13*, 1523–1532.

[22] J. Scheper, M. Guerra-Rebollo, G. Sanclimens, A. Moure, I. Masip, D. González-Ruiz, N. Rubio, B. Crosas, Ó. Meca-Cortés, N. Loukili, V. Plans, A. Morreale, J. Blanco, A. R. Ortiz, À. Messeguer, T. M. Thomson, *PLoS ONE* **2010**, *5*, e11403.

[23] M. M. Hann, A. R. Leach, G. Harper, *J. Chem. Inf. Comput. Sci.* **2001**, *41*, 856–864.

[24] J. M. Holub, H. Jang, K. Kirshenbaum, *Org. Lett.* **2007**, *9*, 3275–3278.

[25] S. B. Y. Shin, B. Yoo, L. J. Todaro, K. Kirshenbaum, *J. Am. Chem. Soc.* **2007**, *129*, 3218–3225.

[26] O. E. Vercillo, C. K. Z. Andrade, L. A. Wessjohann, *Org. Lett.* **2008**, *10*, 205–208.

[27] a) L. Mondragón, M. Orzáez, G. Sanclimens, A. Moure, A. Armiñán, P. Sepulveda, A. Messeguer, M. J. Vicent, E. Pérez-Payá, *J. Med. Chem.* **2008**, *51*, 521–529; b) L. Mondragón, L. Galluzzi, S. Mouhamad, M. Orzáez, J. Vicencio, I. Vitale, A. Moure, A. Messeguer, E. Pérez-Payá, G. Kroemer, *Apoptosis* **2009**, *14*, 182–190.

[28] T. Thomson, J. Scheper, A. Messeguer, Á. Ramirez Ortiz, G. Sanclimens, I. Masip, A. Moure, D. González, A. Morreale, WO/2008/009758, **2008**.

[29] J. Messeguer, I. Masip, M. Montolio, J. A. del Rio, E. Soriano, A. Messeguer, *Tetrahedron* **2010**, *66*, 2444–2454.

[30] The possibility of a hydrogen bond with the second heterocyclic carbonyl group was discarded on the basis of the conformational analysis of **2a**,**b**.

[31] H. Shanan-Atidi, K. H. Bar-Eli, *J. Phys. Chem.* **1970**, *74*, 961–963.

[32] J. Sandstrom in *Dynamic NMR Spectroscopy*, Academic Press, New York, **1982**.

[33] The line-shape simulation was performed by using the gNMR v4.1.0 program.

[34] Free-energy calculations in solution were also performed by running single-point energy determinations by using the standard Poisson–Boltzmann solver included in Jaguar (not reported), although the results did not correlate with the experimental data; clearly, a more accurate solvation treatment, or even calculations with an explicit solvent, would be required to obtain more reliable results, but this was beyond the scope of this study.

[35] a) L. Fielding, *Prog. Nucl. Magn. Reson. Spectrosc.* **2007**, *51*, 219–242; b) B. Meyer, T. Peters, *Angew. Chem.* **2003**, *115*, 890–918; *Angew. Chem. Int. Ed.* **2003**, *42*, 864–890.

[36] SAINT, version 6.22, Bruker AXS Inc., Madison, WI, **2001**.

[37] SADABS, version 2.03, G. M. Sheldrick, University of Göttingen, Göttingen (Germany), **2002**.

[38] SHELXTL, version 6.10, G. M. Sheldrick, Bruker AXS Inc., Madison, WI, **2000**.

[39] Schrödinger, LLC, New York, NY, **2008**.

[40] a) T. A. Halgren, *J. Comput. Chem.* **1999**, *20*, 720–729; b) T. A. Halgren, *J. Comput. Chem.* **1999**, *20*, 730–748.

[41] A. D. Becke, *J. Chem. Phys.* **1993**, *98*, 1372–1377.

[42] C. Lee, W. Yang, R. G. Parr, *Phys. Rev. B* **1988**, *37*, 785–789.

[43] S. Fischer, R. L. Dunbrack, M. Karplus, *J. Am. Chem. Soc.* **1994**, *116*, 11931–11937.

Received: January 20, 2011
Published online: May 24, 2011

